Redox activity of argyrodite Li6PS5Cl electrolyte in all-solid-state Li-ion battery: An XPS study.

Jérémie Auvergniot, Alice Cassel, Dominique Foix, Virginie Viallet, Vincent Seznec, Rémi Dedryvère

Redox activity of argyrodite Li_6PS_5Cl electrolyte in all-solid-state Li-ion battery: an XPS study

Jérémie Auvergniot [a,b], Alice Cassel [b], Dominique Foix [a,c], Virgine Viallet [b,c], Vincent Seznec [b,c,*], Rémi Dedryvère [a,c,*]

[a] IPREM, CNRS UMR 5254, Université de Pau et des Pays de l'Adour
Hélioparc, 2 Avenue Pierre Angot, 64053 Pau Cedex 9, France
[b] LRCS, CNRS UMR 7314, Université de Picardie Jules Verne
33 Rue Saint Leu, 80039 Amiens Cedex, France
[c] Réseau sur le Stockage Electrochimique de l'Energie (RS2E), FR CNRS 3459, France

Abstract

Argyrodite Li_6PS_5Cl is a good candidate as solid electrolyte for bulk all-solid-state Li-ion batteries due to its high ionic conductivity and its good processability, although it shows some interface reactivity towards electrode active materials. In this work we have cycled $LiCoO_2/Li_6PS_5Cl/Li_4Ti_5O_{12}$ full cells and analyzed the interfacial mechanisms by surface-sensitive characterization techniques: Auger Electron Spectroscopy (AES) and X-ray Photoelectron Spectroscopy (XPS). We show that Li_6PS_5Cl has an electrochemical redox activity in the positive electrode. It is partially oxidized into LiCl, P_2S_5 and polysulfides Li_2S_n upon charge, with some reversibility upon discharge. Li_6PS_5Cl also reacts with $LiCoO_2$ upon cycling, leading to the formation of phosphates at the interface.

Keywords: all-solid-state Li-ion battery, solid electrolyte, argyrodite Li_6PS_5Cl, electrode/electrolyte interfaces, XPS, Auger

* Corresponding authors: remi.dedryvere@univ-pau.fr, vincent.seznec@u-picardie.fr

1. Introduction

Lithium ion battery technology is currently the most attractive power source for mobile devices because of its high energy density and long cycle life. Organic liquid electrolytes used in common Li-ion batteries pose several safety issues, such as risks of electrolyte leakage, fire and explosion. [1,2] To solve this problem, "all-solid-state" batteries using a non-flammable solid electrolyte have been recognized and developed as a safer alternative. [3,4,5,6,7] Historically, solid electrolytes have not been used much in bulk batteries until recently because of a lower ionic conductivity than organic liquid electrolytes at room temperature. However, in 2011 Kanno *et al.* [3] reported on a new solid electrolyte $Li_{10}GeP_2S_{12}$ showing a high conductivity of $1.2x10^{-2}$ $S.cm^{-1}$ at 25°C, which is comparable or higher than standard organic liquid electrolytes at room temperature. In 2008 Deiseroth *et al.* [8] reported on Li-containing argyrodites of general formula $Li_{7-x}PS_{6-x}X_x$ ($0 \leq x \leq 1$, X = Cl, Br, I) with high Li^+ ion conductivities. Pecher *et al.* [9] reported values close to $4x10^{-7}$ $S.cm^{-1}$ for Li_6PS_5I. Rao *et al.* reported high ionic conductivities of $3x10^{-3}$ $S.cm^{-1}$ and $7x10^{-3}$ at 25°C for Li_6PS_5Cl and Li_6PS_5Br respectively, which were both prepared through mechanical milling followed by an annealing of 5h at 550°C. [10] Boulineau *et al.* obtained a $1.33x10^{-3}$ $S.cm^{-1}$ conductivity with a Li_6PS_5Cl phase that was synthetized through a simple 10h ball-milling. [2]

Li_6PS_5Cl and Li_6PS_5Br argyrodites have been used in all-solid-state batteries by several groups, showing promising results both in Li-ion systems and Li-S systems. [11,11,12,13,14,15] However, rapid capacity loss has been observed in $LiCoO_2/Li_6PS_5Cl/Li_4Ti_5O_{12}$ full cells, which was investigated by an arsenal of techniques such as Electrochemical Impedance Spectroscopy, XRD, DSC, TGA or even SEM. No definitive answers were given from those techniques regarding capacity loss, which was suspected to be coming from the positive electrode. [15] Yu *et al.* also observed a rapid capacity fading in $S\text{-}C/Li_6PS_5Cl/Li\text{-}In$ all-solid-state lithium-sulfur batteries and concluded from impedance measurements that the capacity fading is due to an increase of the electrode-electrolyte interface resistance. [16]

The aim of the present paper is to focus on the mechanisms occurring at interfaces between argyrodite and active materials ($LiCoO_2$ and $Li_4Ti_5O_{12}$) in order to identify the reasons for capacity fading. $LiCoO_2/Li_6PS_5Cl/Li_4Ti_5O_{12}$ all-solid-state batteries were electrochemically cycled and then the composite electrodes were analyzed by surface-

sensitive characterization techniques: Auger Electron Spectroscopy (AES) and X-ray Photoelectron Spectroscopy (XPS).

2. Experimental section

Argyrodite Li_6PS_5Cl was synthesized from the reagents Li_2S (Sigma Aldrich 99%), P_2S_5 (Sigma Aldrich 99%) and LiCl (Acros Organic 99%) by ball-miling at 600 rpm for 10h under argon atmosphere. Argyrodite was used as solid electrolyte in all-solid state $LiCoO_2/Li_6PS_5Cl/Li_4Ti_5O_{12}$ full cells. Both the positive and negative electrodes were formulated with 38 wt.% of active material, 57 wt.% of solid electrolyte, 5 wt.% of carbon fibers (VGCF) as conducting additive. The components were mixed by grinding in an agate mortar. The mass ratio of composite electrodes was chosen as follows: 10mg of positive electrode ($LiCoO_2$) vs. 20 mg of the negative electrode ($Li_4Ti_5O_{12}$) so that the negative electrode was in excess. The two electrodes were separated by an electrolyte layer containing only argyrodite. The thickness of the resulting battery was about 800 µm. Galvanostatic cycling was carried out at room temperature between 1 V and 2.6 V at a C/10 rate, which means that one Li^+ per $LiCoO_2$ unit is exchanged in 10 h.

Auger Electron Spectroscopy (AES) analysis was performed with a JEOL JAMP 9500F Auger Spectrometer (JEOL Ltd, Tokyo, Japan) also used for Scanning Electron Microscopy (SEM). AES spectra were recorded between 50 and 800 eV kinetic energy in constant retarding ratio (CRR) mode with $\Delta E/E = 0.5\%$ at a working distance of 23 mm, with a 10 kV potential and a 1 nA current. The pressure was lower than $2x10^{-7}$ Pa. SEM images were obtained in the same conditions.

X-ray Photoelectron Spectroscopy (XPS) was carried out with a Kratos Axis Ultra spectrometer using a focused monochromatized Al Kα radiation (hν = 1486.6 eV). Repeatability of the analysis has been systematically tested by using multiple spots of every sample. The non-degradation of the samples under the X-ray beam was checked by recording different spectra of the same sample at different times. The analyzed area of the samples was 300×700 µm^2. Peaks were recorded with a constant pass energy of 20 eV. The binding energy scale was calibrated from the hydrocarbon contamination using the C 1s peak at 285.0 eV. For all analyses, thorough precautions were taken to preserve the samples

surface from contact with air and moisture. All samples were handled or stored in dry argon atmosphere. The XPS introduction chamber was directly connected to the argon glovebox. For AES a vacuum transfer chamber was used.

For AES and SEM analyses, the battery was manually broken into two parts in the argon glovebox in order to access its cross-section. For XPS measurements the unbroken battery was put on an adhesive tape and then mechanically etched with a scalpel until the core of the electrode was reached. To analyze the electrolyte part of the battery, the same process was used by removing completely the negative electrode side until the core of the electrolyte was reached. No argon ion sputtering was used to etch the samples surface, in order to avoid any ion beam-induced chemical changes.

3. Results and discussions

3.1. Characterization of pristine electrodes

The bulk all-solid-state battery architecture is shown in Figure 1. Both composite electrodes consist of a mixture of active material, argyrodite and carbon fibers. Between the electrodes, there is only argyrodite and this part will be called the solid electrolyte hereafter. The AES spectra of $LiCoO_2$ (LCO), $Li_4Ti_5O_{12}$ (LTO) and Li_6PS_5Cl (Arg) particles, respectively, observed on a battery cross section are represented in Figure 2. Each phase can be distinguished from the other ones by a characteristic Auger peak. Ti LMM (380 eV) is the signature of LTO, Co LMM (650-800 eV) is the signature of LCO, and S LVV (150 eV) is characteristic of the argyrodite phase. The presence of a small S LVV peak in the spectra of LTO and LCO comes from a small amount of argyrodite at the surface of the particle (composite electrode). The presence of a small C KVV peak is due either to neighbouring carbon fibers or to carbon surface contamination.

Scanning Auger Microscopy (SAM) mapping of C, S, Ti and Co elements and SEM images of a cross-section of the negative and positive electrodes are shown in Figure 3 and Figure 4, respectively. Intensity contrast between C, Co, Ti and S elements in SAM images allows us to visualize the active materials particles, the argyrodite and the carbon fibers. In the negative electrode we can see that the LTO particles are smaller than the argyrodite particles (Figure 3). In the positive electrode the LCO particles are quite large ($d > 10\mu m$) (Figure 4).

3.2. Electrochemical cycling

The LCO / Li_6PS_5Cl / LTO full cell was cycled at a C/10 rate between 1.0 and 2.6 V. Figure 5 shows the voltage vs. capacity galvanostatic curves, and the capacity retention vs. cycle number.

We can observe in Figure 5 that the battery has an initial discharge capacity of 66 mAh/g (of LCO). Afterwards its capacity rapidly drops and the battery loses 50% of its discharge capacity after 9 cycles only. Our aim in this paper is to understand the origin of this important loss of performance upon cycling. Therefore we investigated the three different parts of the electrode (i.e. the positive electrode, the negative one and the electrolyte) by XPS. The analyses were carried out on the pristine battery, after one cycle, and post-mortem (after 45 cycles).

3.3. XPS characterization after cycling

Ti 2p XPS spectra of the negative electrode part are shown in Figure 6. The spectrum of the pristine electrode is split in two parts due to spin-orbit coupling, with an area ratio of about 2/1. The Ti $2p_{3/2}$ component is observed at 458.6 eV and the Ti $2p_{1/2}$ at 464.4 eV, corresponding to Ti^{4+} ions in an oxygen environment, in good agreement with previous studies on LTO active material. [17] No significant changes can be observed after one cycle.

After 45 cycles and the complete loss of capacity, however, an additional Ti environment is observed at a binding energy (BE) of 456.8 eV, which is characteristic of Ti^{3+}. This additional peak is repeated in the $2p_{1/2}$ part of the spectrum. This peak corresponds to the lithiated phase $Li_7Ti_5O_{12}$, and has also been observed in previous studies. [18] As a result, the negative electrode still remains in a partially charged state in the post mortem battery, whereas it is supposed to be in a discharged state. This observation highlights reversibility issues of the battery.

Co $2p_{3/2}$ XPS spectra of the positive electrode at the same stages (pristine, 1 cycle, 45 cycles) are reported in Figure 7. The spectrum of the pristine electrode consists of an asymmetric main peak at BE = 779.8 eV and “shake up” satellite at +10 eV, as expected for LCO. After one cycle, and especially after 45 cycles, the spectrum shape changes: the main peak is broadened and its asymmetry towards highest BE increases. Now, variations of Co 2p

peak as a function of Co oxidation state are very subtle. It was shown in a previous work [19] that the oxidation of Co^{3+} ions in Li_xCoO_2 upon charge (delithiation) results in broadening and increase of the asymmetry of the Co 2p main peak, and in decrease of the satellite to main peak intensity ratio, with no clear BE shift of the main peak. Therefore an interesting comparison can be made with the Co $2p_{3/2}$ spectrum of a Li_xCoO_2 sample that was delithiated in a standard Li-ion cell, *i.e.* with a liquid electrolyte, which is represented by the dashed red line in Figure 7 ($Li_{0.7}CoO_2$). [19] The shape of the main peak is rather similar (broadening and asymmetry) for this sample and for our LCO/argyrodite electrode after 45 cycles. However, the overall spectrum shape is not exactly the same because the Co 2p spectrum of the LCO/argyrodite electrode displays some additional intensity in the 784-788 eV BE region. Therefore the shape of Co 2p spectra we observe after cycling is not clearly explained and may be due to the contribution of several cobalt environments. So it could be due to chemical reactivity of LCO towards argyrodite at the interface. Note that the reactivity of LCO towards a sulfur-based solid electrolyte was already reported by Sakuda *et al*. [20,21] Indeed, they observed by EDX the diffusion of Co, S and P elements at the interface between LCO and Li_2S-P_2S_5. Moreover, a recent theoretical study (DFT-GGA) of the interface stability of solid electrolytes towards active materials predicts the formation of $Co(PO_3)_2$ and CoS_2 at the interface between LCO and Li_3PS_4. [22]

In order to better understand the interfacial reactivity of argyrodite, we carefully analyzed Cl 2p, Li 1s, S 2p and P 2p XPS core peaks. As argyrodite is present in all parts of the battery (positive and negative electrodes, solid electrolyte), its XPS spectra in each part are shown.

The Cl 2p spectra (Figure 8) show a unique 3/2-1/2 doublet (Cl $2p_{3/2}$ at 198.8 eV) characteristic of Cl^- ions of argyrodite [23] in all parts of the battery and at any stage of cycling. Therefore no chemical change of chlorine can be evidenced, which remains as Cl^- ions.

The case is different for Li 1s spectra, which are reported in Figure 9. Note that in the Li 1s spectra of the composite electrodes the contribution of lithium from argyrodite is dominant because of the proportion of solid electrolyte is 57 wt.%. In the negative electrode part and in the solid electrolyte part of the battery the Li 1s signature of argyrodite does not change upon cycling (BE = 55.6 eV). However, in the positive electrode part an additional Li 1s

component is observed after 45 cycles (BE = 56.4 eV). This component is clearly attributed to LiCl [23], which was confirmed in this work by the XPS analysis of a LiCl commercial reference that presented a Cl 2p peak at 198.8 eV, and a Li 1s peak at 56.4 eV. Note that LiCl could not be detected in the Cl 2p spectra (Figure 8) because its Cl 2p BE is about the same as argyrodite.

Investigation of P 2p spectra is reported in Figure 10. For phosphorus as well the P 2p signature of argyrogite (BE $2p_{3/2}$ = 132.0 eV) does not change upon cycling in the negative electrode and in the solid electrolyte part of the battery. In the positive electrode, however, additional components are observed after cycling. After 45 cycles two additional 3/2-1/2 doublets are necessary to fit the spectrum shape. The first one at BE = 132.9 eV is in good agreement with phosphorus from P_2S_5 [24], which was confirmed by an internal reference in the lab. This P_2S_5 component was also necessary to fit correctly the P 2p spectrum obtained after only one cycle, but with much smaller intensity. After 45 cycles the additional P 2p component at higher BE (134.0 eV) can be assigned to phosphorus atoms in a more oxidized environment (phosphate), which could be due to the reaction of argyrodite with oxygen during cycling. The origin of this oxygen, however, will be discussed after comments on the S 2p spectra.

The analysis of S 2p spectra was very rich in information, as shown in Figure 11. The S 2p spectrum of argyrodite consists of a S $2p_{3/2-1/2}$ doublet with S $2p_{3/2}$ at BE = 161.7 eV (red component). In the pristine battery an additional weak doublet at 160.5 eV (brown in figure 11) can be attributed to Li_2S and corresponds to remaining traces of this reagent used for the synthesis of argyrodite (this was also confirmed by X-ray diffraction data, not shown here). A third weak component at 167.1 eV can hardly be detected. It is explained by traces of sulfite environment (SO_3^{2-}) at the surface. In the negative electrode part and in the solid electrolyte part of the battery, the S 2p spectra do not change after cycling, except for the presence of an increased amount of sulfite at the surface. In the positive electrode part, the spectra is significantly modified, especially after 45 cycles. First, the signature of Li_2S disappears. Secondly, two additional S 2p doublets appear in the spectrum, with S $2p_{3/2}$ at BE = 162.1 eV and 163.5 eV, respectively. The first one at 162.1 eV (yellow in Figure 11) can be assigned to terminal sulfur atoms of P_2S_5 (P=S groups). However, its relative intensity compared to the corresponding P 2p component is too high so it cannot be assigned solely

to P_2S_5. The second new component at 163.5 eV (orange in Figure 11) is in good agreement with the BE observed for bridging sulfur atoms of P_2S_5 (P-S-P groups). However, its relative intensity is too large as well and it cannot be assigned solely to P_2S_5 either. Therefore an extra sulfur-containing compound is present after one cycle and after 45 cycles. To understand the origin of this compound, an interesting comparison with lithium-sulfur (Li-S) batteries should be made. In Li-S batteries, Li_2S is converted into polysulfides (Li_2S_n) upon charge (oxidation) of the sulfur electrode. [25] In our case we can observe in Figure 11 that the Li_2S initially present in the argyrodite disappears after 45 cycles only in the positive electrode side, which is certainly due to oxidation process upon charge. Since the additional component observed at 163.5 eV is perfectly consistent with the BE of bridging sulfur atoms of Li_2S_n [26], this means that Li_2S is oxidized into polysulfides in the positive electrode upon cycling (oxidation upon charge). Moreover, the component attributed to Li_2S_n is already observed after one cycle in Figure 11, whereas Li_2S is still present at this stage. This suggests that argyrodite is also partially oxidized into polysulfides Li_2S_n. Moreover, this assumption is in good agreement with the partial decomposition of argyrodite into LiCl and P_2S_5 in the positive electrode, as shown by P 2p and Li 1s spectra. The formation of pure P_2S_5 (*i.e.* P_4S_{10} molecules) by oxidation of Li_6PS_5Cl is rather unlikely. The formation of a disordered "P_2S_5" compound containing bridging and terminal sulfur atoms is more probable.

Concerning the presence of oxygen in the environment of sulfur and phosphorus upon cycling, there is an interesting difference between those two elements. Indeed, traces of sulfite environment are detected at the surface of argyrodite in all parts of the battery (BE at 167.1 eV, green component). It seems to be due to the reaction of argyrodite with traces of oxygen in the battery. The amount of sulfite roughly increases vs. cycle number probably due to increasing time. The presence of oxygen in the environment of phosphorus, however, is detected only in the positive electrode after 45 cycles (as seen in Figure 10) while this sample contains less sulfite than the negative electrode or the electrolyte. This means that the reaction of phosphorus with oxygen does not originate from the same process as the formation of sulfite. It results from an electrochemical process within the positive electrode during charge. The main source of oxygen in the positive electrode is of course the active material LCO. In our cycling conditions the voltage reached 2.6 V vs. LTO, which is about 4.15 V vs. Li^+/Li. This potential is not very high for LCO, which is not expected to release

oxygen spontaneously in these conditions. However an interfacial reactivity of argyrodite towards LCO is possible since it was already evidenced for Li_2S-P_2S_5 electrolyte. [20] The formation of phosphates at the interface is also in good agreement with the study of Visbal *et al.* [27] who detected by Time-of-Flight Secondary Ion Mass Spectrometry (ToF-SIMS) the presence of PO_3^- and PO_4^- ions at the interface between $LiNi_{0.8}Co_{0.15}Al_{0.05}O_2$ and Li_2S-P_2S_5 after 100 cycles. In our case argyrodite reacts with LCO upon charge, and the presence of phosphates is detected by XPS only after repeated cycling.

In order to confirm the partial oxidation of argyrodite into LiCl, "P_2S_5" and polysulfides Li_2S_n in the positive electrode upon charge, we carried out an additional experiment. Argyrodite was used as active material in a Li_6PS_5Cl/Li-In half-cell, in which a lithium-indium alloy (6 wt.% of Li) was used as counter electrode. Argyrodite was mixed with Ketjen Black (33 wt.%) for electronic conductivity. The cycling conditions were the same as full cells (C/10). The half-cell was stopped during the first charge up to 3.5 V vs. Li-In, which is equivalent to 4.1 V vs. Li^+/Li [28,29], and the argyrodite electrode was kept in this charged state for XPS analysis. S 2p and P 2p XPS spectra of the charged argyrodite electrode are shown in Figure 12. In the S 2p spectrum, we can observe exactly the same components as for the LCO composite electrode after cycling. The Li_2S component also disappears. In the P 2p spectrum, the component attributed to P_2S_5 can be observed as well, but the component assigned to phosphates is not detected, certainly due to the absence of LCO. The intensity ratio between S 2p and P 2p peaks requires that both P_2S_5 and Li_2S_n are present. This experiment proves the electrochemical activity of argyrodite and its sensitivity towards oxidation in the positive electrode. Note that the amounts of P_2S_5 and Li_2S_n obtained after a first charge are greater after a first charge of the Li_6PS_5Cl/Li-In half-cell than after a complete cycle of a $LiCoO_2$/Li_6PS_5Cl/$Li_4Ti_5O_{12}$ full cell, therefore a possible reversibility of the oxidation process of argyrodite can be suspected upon discharge.

Han *et al.* also evidenced an electrochemical activity for the $Li_{10}GeP_2S_{12}$ phase. [30] In their work they even demonstrated the possibility of cycling a full cell made from $Li_{10}GeP_2S_{12}$ as single material playing the three roles of cathode, anode and solid electrolyte. Tarhouchi *et al.* reported the same kind of electrochemical activity for the $Li_{10}SnP_2S_{12}$ phase and demonstrated that the same material could be used as negative electrode and solid electrolyte in a $LiCoO_2$ / $Li_{10}SnP_2S_{12}$ / $Li_{10}SnP_2S_{12}$-C full cell. [31] In our case, we show by XPS

the anodic reactivity of argyrodite Li_6PS_5Cl in the battery upon cycling. XPS was already used by Wenzel *et al.* [32,33] to identify the products of cathodic reactivity of $Li_7P_3S_{11}$ solid electrolyte towards lithium. They identified Li_2S and Li_3P formed at the $Li_7P_3S_{11}$ / Li interface. For the anodic reactivity of argyrodite we propose the reaction scheme described by Equation (1). Upon charge, argyrodite is oxidized in the positive electrode and a fraction of lithium is extracted from the Li_6PS_5Cl phase. As a result, it is partially decomposed into LiCl, "P_2S_5" and Li_2S_n with an undetermined polysulfide average chain length n.

$$Li_6PS_5Cl \rightarrow LiCl + \frac{1}{2}P_2S_5 + \frac{5}{2n}Li_2S_n + 5\left(1-\frac{1}{n}\right)Li^+ + 5\left(1-\frac{1}{n}\right)e^- \quad (1)$$

This mechanism occurs only at the interface with $LiCoO_2$ particles or conductive carbon additive (VGCF here), *i.e.* where the exchange of electrons is possible. Additionally, the reactivity of argyrodite towards $LiCoO_2$ upon charge can be evidenced, which is observed after repeated cycles. The partial degradation of argyrodite may explain the loss of reversible capacity observed upon cycling (as shown in Figure 5). The charge-discharge voltage profiles display a gradual loss of exchangeable lithium. The reason is that a fraction of Li^+ ions that are inserted into LTO are coming from the electrochemical oxidation of argyrodite, which constitutes 57 wt.% of the electrode composition, instead of coming from LCO. As the oxidation process of argyrodite is not completely reversible, the Li^+ ions cannot be fully extracted from LTO upon discharge. The interfacial reactivity between LCO and argyrodite may also play a role in the loss of capacity.

4. Conclusion

In this work, we have cycled LCO / Li_6PS_5Cl / LTO full cells. XPS analysis of both electrodes, which contain Li_6PS_5Cl in their formulation, has shown that the negative electrode material LTO still remains in a charged state after cycling (end of discharge of the battery). Argyrodite undergoes no chemical or electrochemical degradation in the composite negative electrode, but on the contrary is partially decomposed into LiCl, P_2S_5 and polysulfides in the positive electrode. Additionally, argyrodite shows an interfacial reactivity with LCO to form a phosphate environment upon cycling, that is not related to the reaction with traces of oxygen coming from outside the battery. Complementary cycling of a Li_6PS_5Cl/Li-In half-cell has shown that this electrochemical oxidation of argyrodite can be observed as soon as the

first charge. It is partially reversible upon discharge. This interfacial electrochemical and chemical reactivity of argyrodite in the positive electrode may be modified by the use of an inorganic coating (for example $LiNbO_3$) on $LiCoO_2$ since it was shown that the coating allows reducing interfacial resistances within the positive electrode. [34] The appearance of an insulating phase like LiCl at the interface between the active material and the solid electrolyte may be the reason for interfacial impedance increase, such as suggested by previous studies. [16] However electrochemical activity of argyrodite does not necessarily exclude this material as solid electrolyte if the redox processes are reversible. Further work will be conducted to determine the reactivity of argyrodite towards other positive electrode active materials with different working potentials to evaluate the possibility to use it as solid electrolyte in all-solid-state batteries.

Acknowledgments:

The authors thank the French National Research Agency (ANR) for financial support of Labex STORE-EX (ANR-10-LABX-0076).

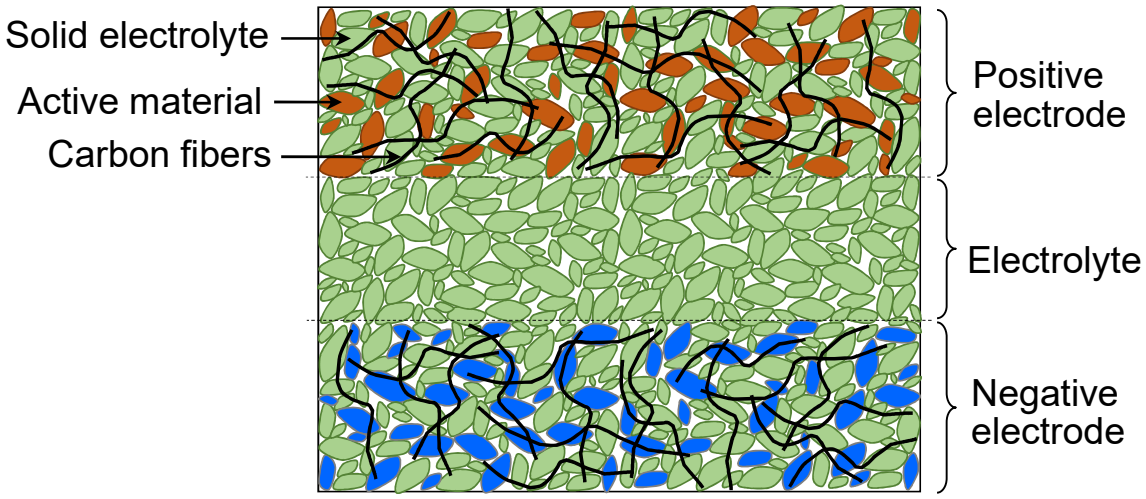

Figure 1: Schematic view of a cross-section of the all-solid-state battery studied in this work

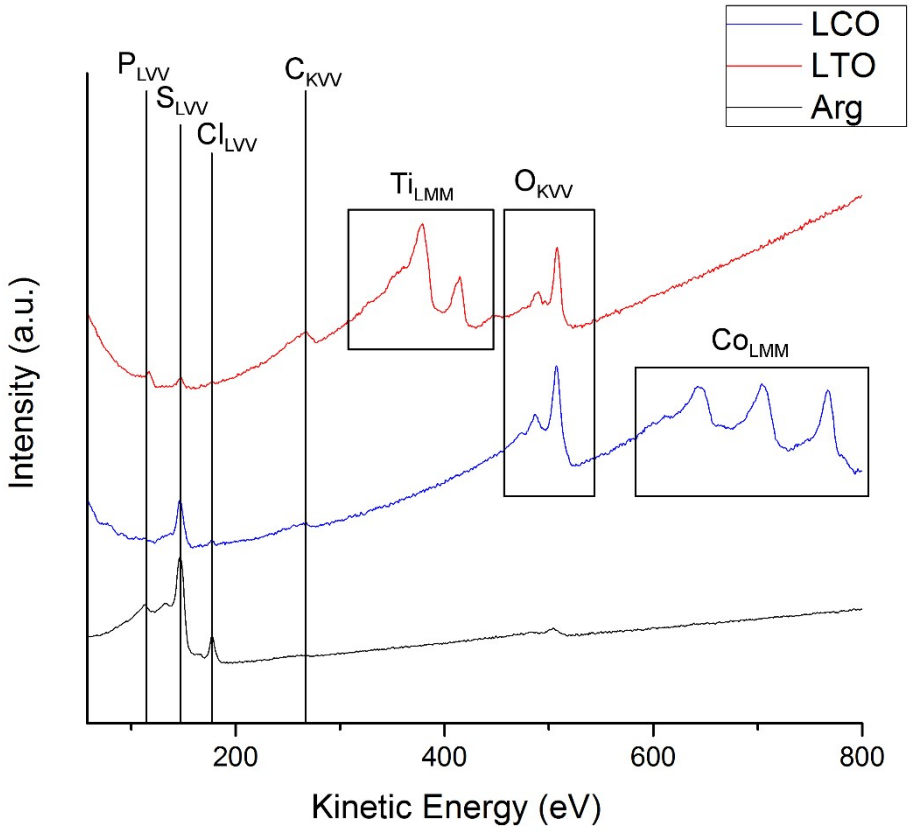

Figure 2: AES spectra of a LCO particle (in blue), of a LTO particle (in red) and of an argyrodite particle (in black) obtained on a cross-section of the battery.

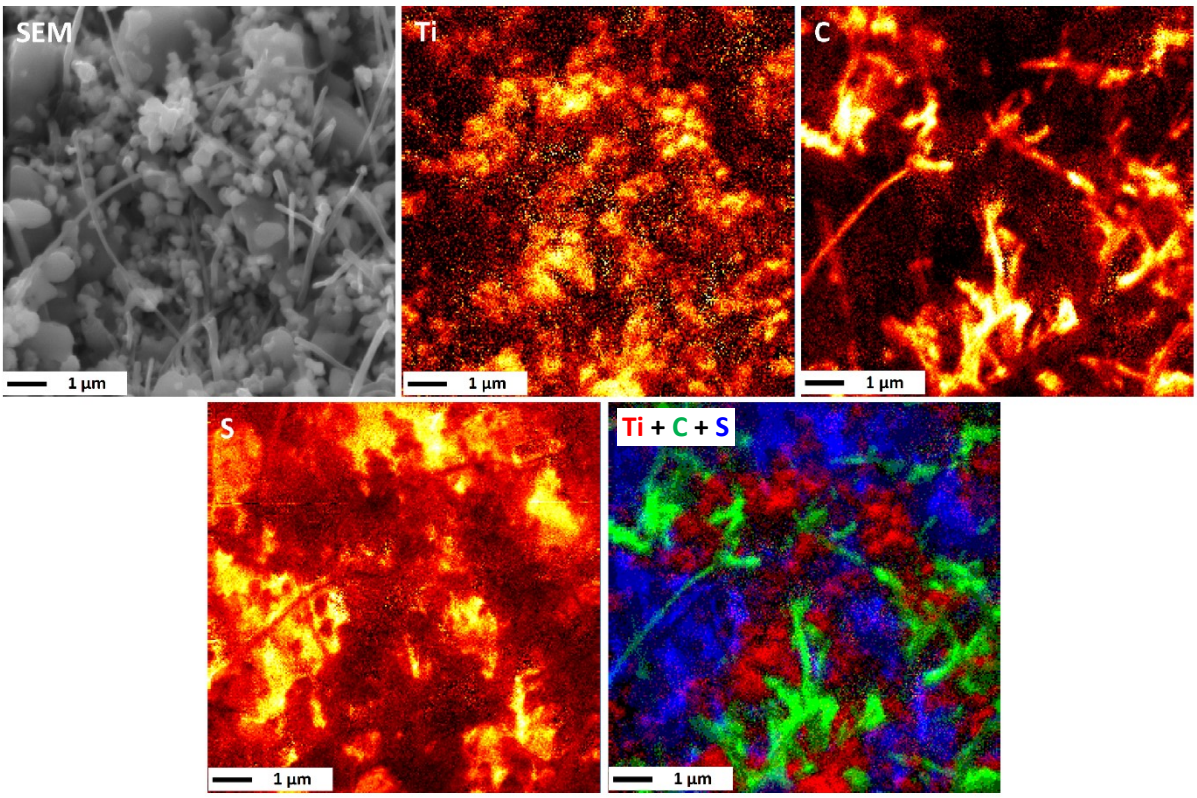

Figure 3: **a)** SEM image of the negative electrode. **b)**, **c)**, **d)** SAM mapping of the elements Ti, C and S respectively. **e)** SAM mapping of Ti (in red), C (in green) and S (in blue). (Bar = 1µm)

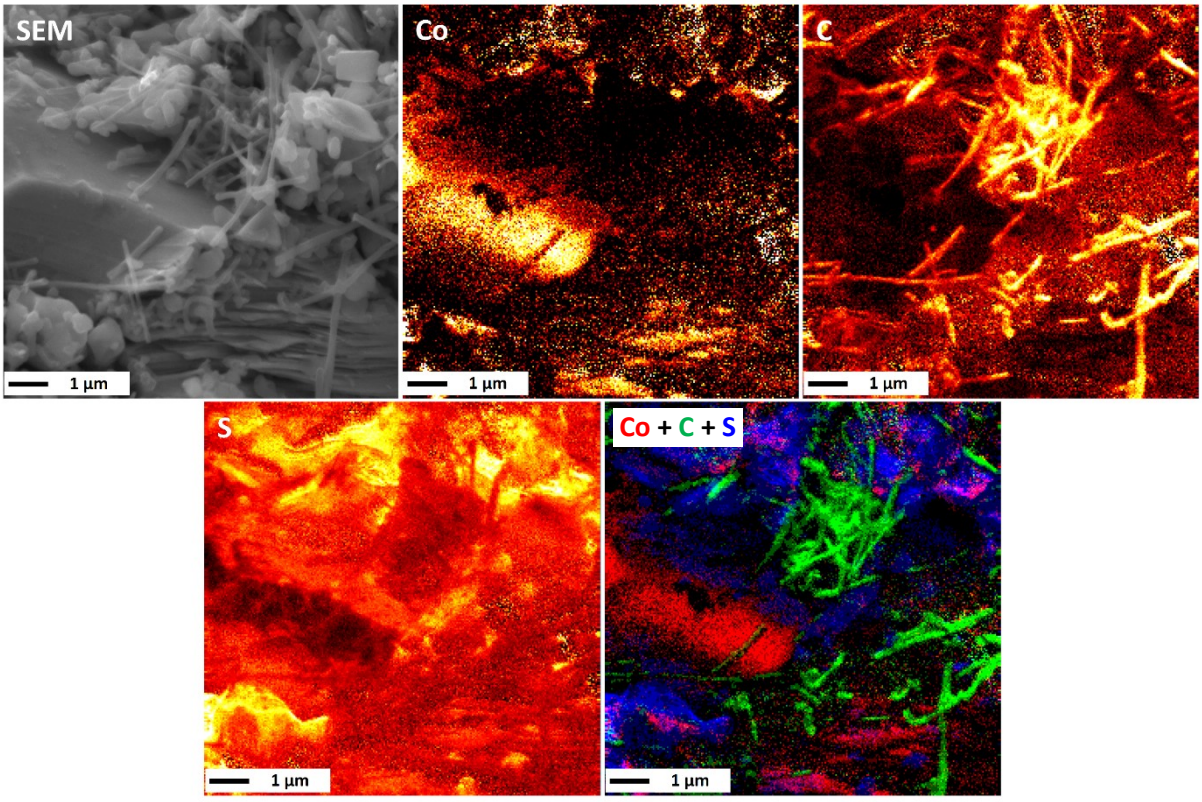

Figure 4: **a)** SEM image of the positive electrode. **b)**, **c)**, **d)** SAM mapping of the elements Co, C and S respectively. **e)** SAM mapping of Co (in red), C (in green) and S (in blue). (Bar = 1µm)

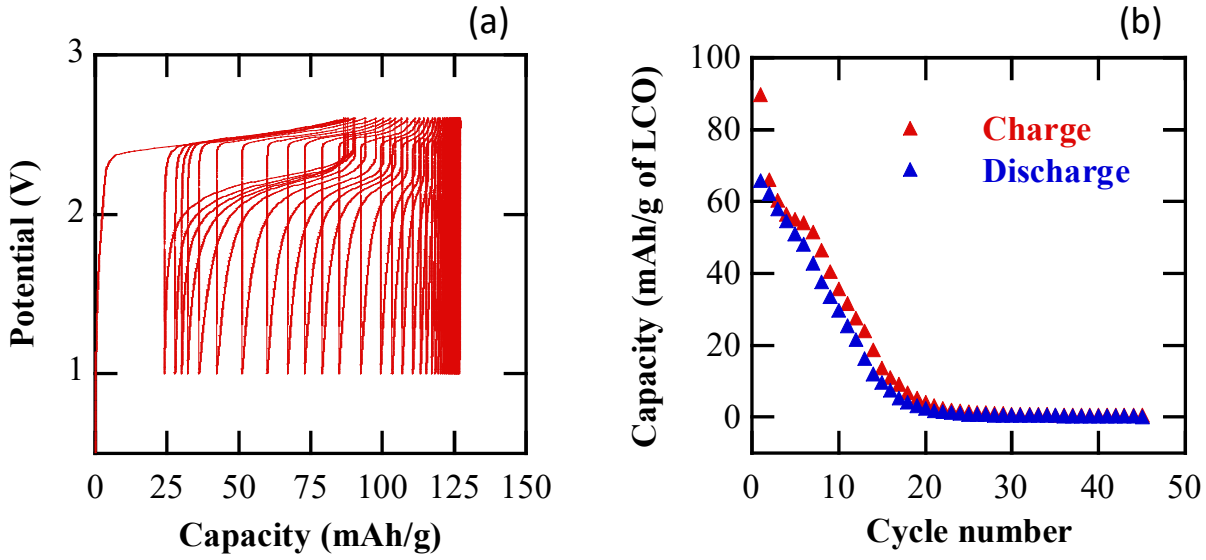

Figure 5: Electrochemical behaviour of a LCO / Li_6PS_5Cl /LTO full cell cycled between 1.0 and 2.6 V at 20°C and a C/10 rate. **a)** Charge-discharge voltage profiles. **b)** Capacity retention vs. cycle number.

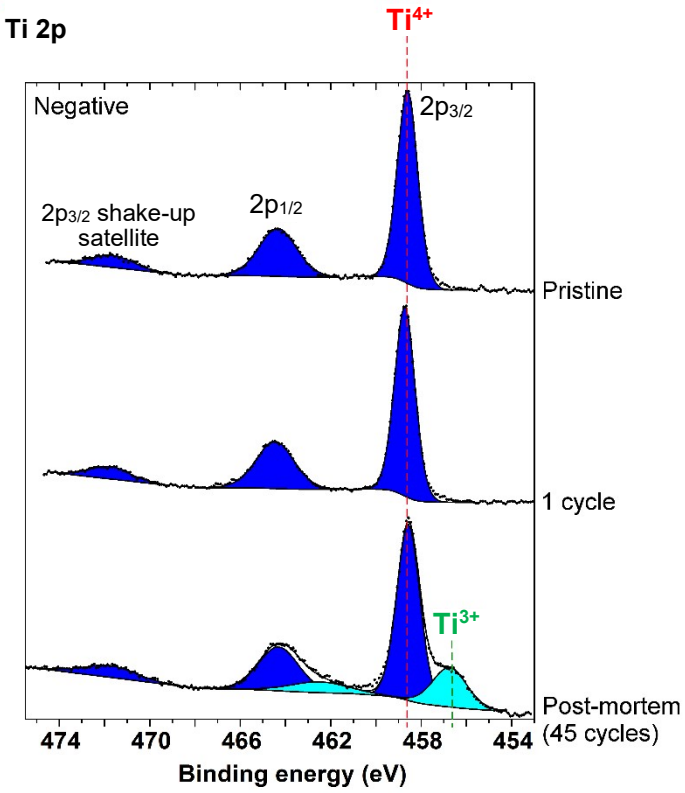

Figure 6: Ti 2p XPS spectra from the negative electrode (LTO) part of the LCO / Li_6PS_5Cl /LTO battery, before cycling (pristine), after one cycle and after 45 cycles (post-mortem).

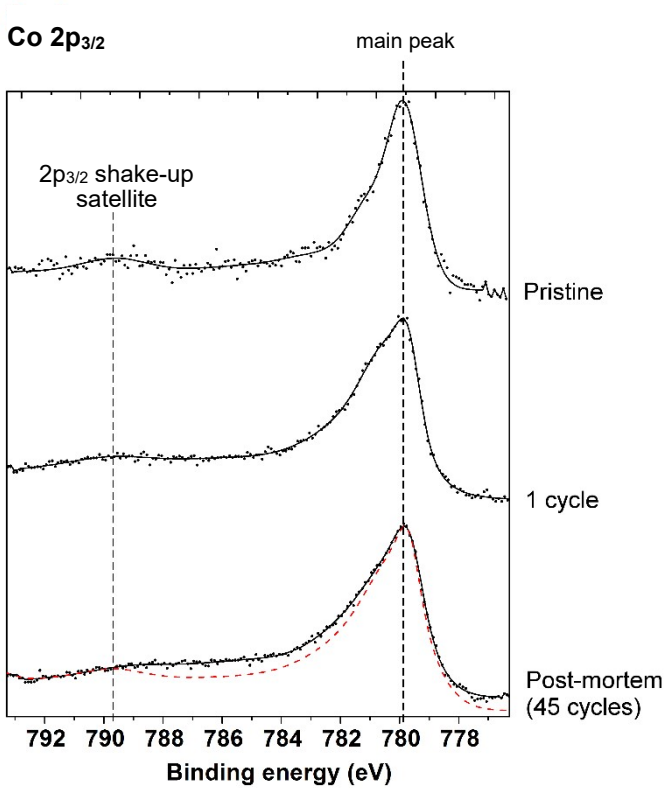

Figure 7: Co $2p_{3/2}$ XPS spectra from the positive electrode (LCO) part of the battery, before cycling (pristine), after one cycle and after 45 cycles (post-mortem). Dashed red line corresponds to a Li_xCoO_2 electrode (x=0.7) delithiated in a standard Li-ion cell (adapted with permission from Dahéron et al.[19] Copyright 2008 American Chemical Society)

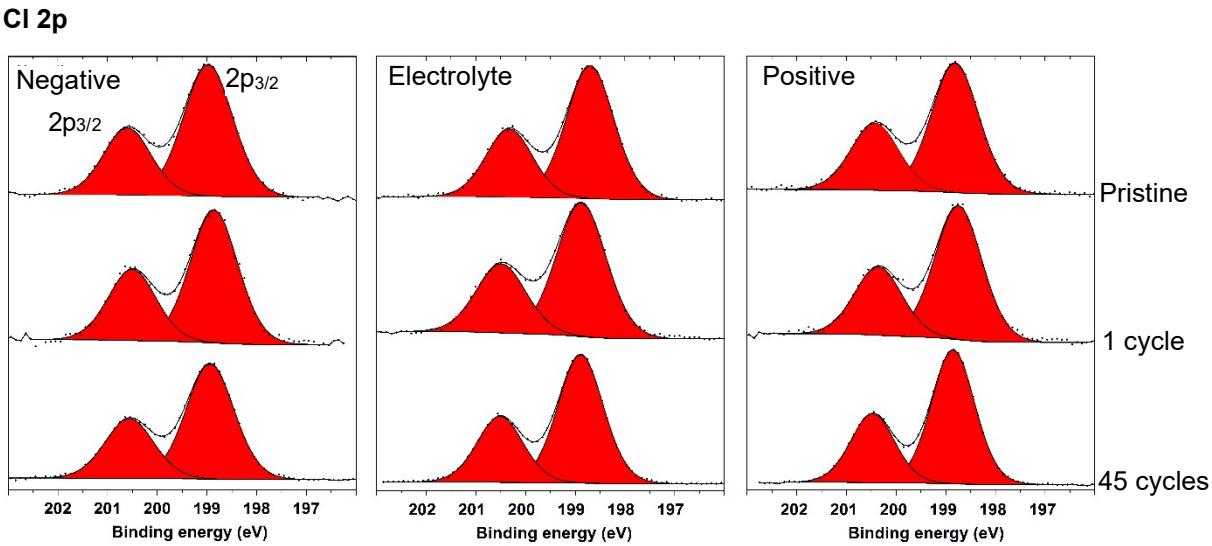

Figure 8: Cl 2p XPS spectra of the three parts of the LCO / Li_6PS_5Cl /LTO battery (positive and negative electrodes, solid electrolyte): before cycling (pristine), after one cycle and after 45 cycles (post-mortem).

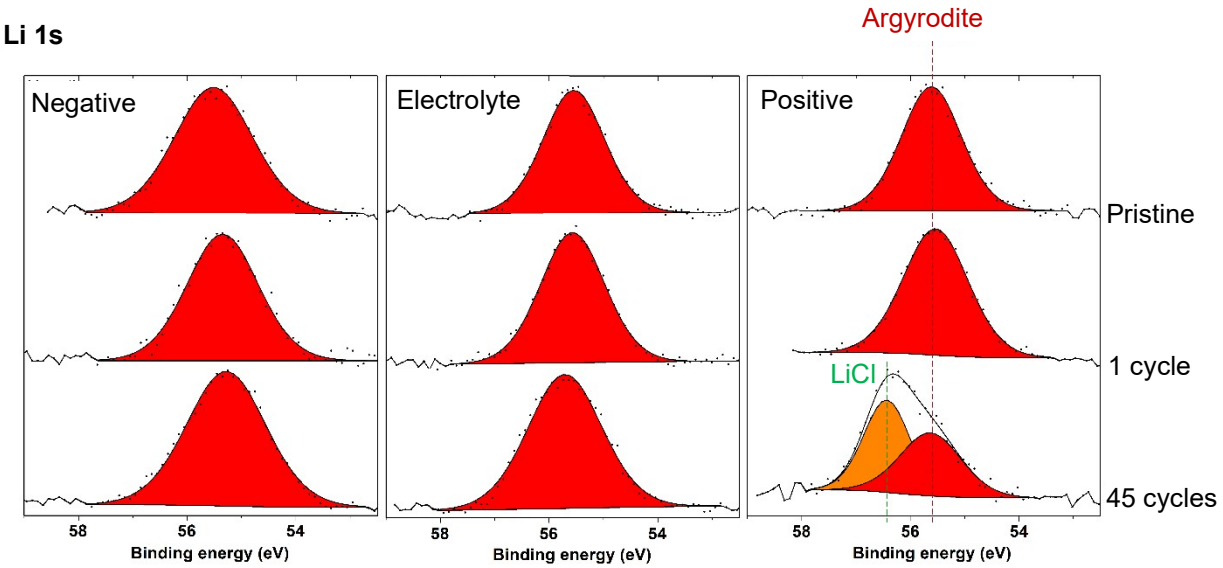

Figure 9: Li 1s XPS spectra of the three parts of the battery (positive and negative electrodes, solid electrolyte): before cycling (pristine), after one cycle and after 45 cycles (post-mortem).

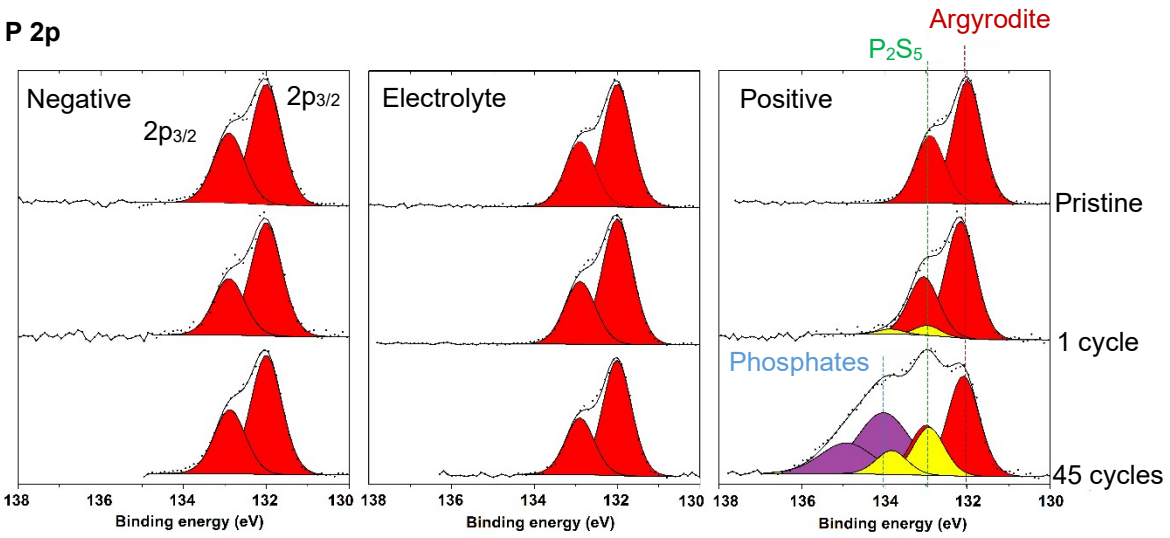

Figure 10: P 2p XPS spectra of the three parts of the battery (positive and negative electrodes, solid electrolyte): before cycling (pristine), after one cycle and after 45 cycles (post-mortem).

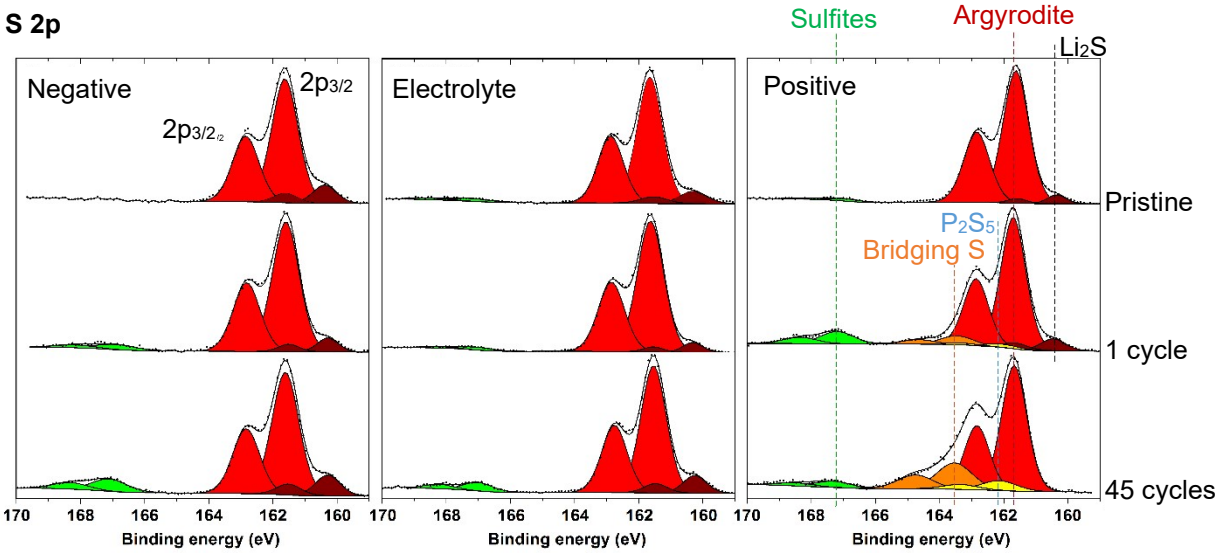

Figure 11: S 2p XPS spectra of the three parts of the battery (positive and negative electrodes, solid electrolyte): before cycling (pristine), after one cycle and after 45 cycles (post-mortem).

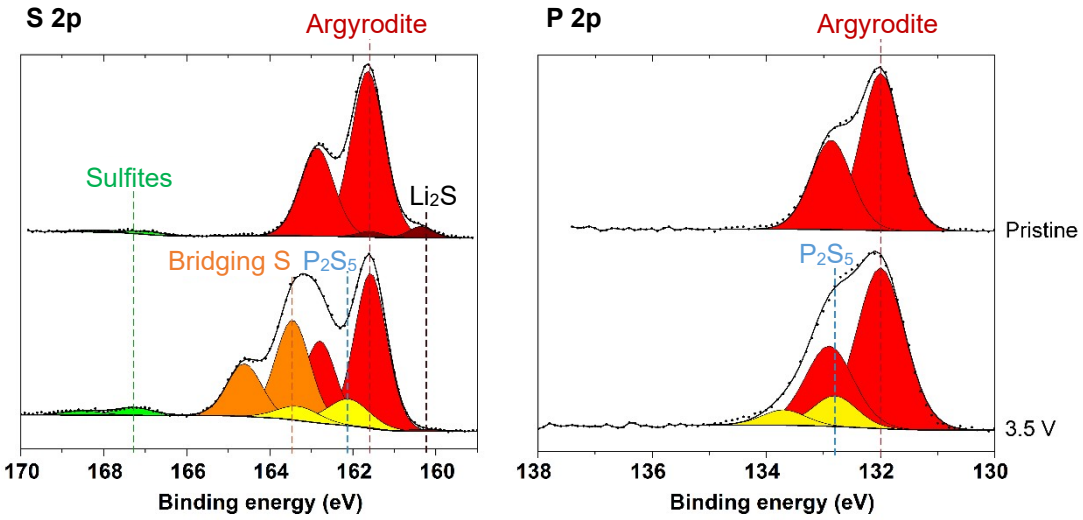

Figure 12: S 2p and P 2p XPS spectra of argyrodite electrode after charge of a Li_6PS_5Cl/Li-In half-cell up to 3.5 V. Comparison with the pristine argyrodite electrode.

References

[1] Fergus, J. W. J. Power Sources 2010, 195, 4554-4569.

[2] Boulineau, S.; Courty, M.; Tarascon, J.-M.; Viallet, V. Solid State Ionics 2012, 221, 1–5.

[3] Kamaya, N.; Homma, K.; Yamakawa, Y.; Hirayama, M.; Kanno, R.; Yonemura, M.; Kamiyama, T.; Kato, Y.; Hama, S.; Kawamoto, K.; Mitsui, A. Nat. Mater. 2011, 10, 682–686.

[4] Birke, P.; Salam, F.; Döring, S.; Weppner, W. Solid State Ionics 1999, 118, 149–157.

[5] Aboulaich, A.; Bouchet, R.; Delaizir, G.; Seznec, V.; Tortet, L.; Morcrette, M.; Rozier, P.; Tarascon, J.-M.; Viallet, V.; Dollé, M. Adv. Energy Mater. 2011, 1, 179–183.

[6] Mizuno, F.; Hayashi, A.; Tadanaga, K.; Tatsumisago, M. Advanced Materials, 2005, 17, 918-921

[7] Chen, M.; Prasada Rao, R.; Adams, S. Solid State Ionics 2014, 268, 300–304.

[8] Deiseroth, H.-J.; Kong, S.-T.; Eckert, H.; Vannahme, J.; Reiner, C.; Zaiss, T.; Schlosser, M. Angew. Chemie 2008, 47, 755–758.

[9] Pecher, O.; Kong, S. T.; Goebel, T.; Nickel, V.; Weichert, K.; Reiner, C.; Deiseroth, H. J.; Maier, J.; Haarmann, F.; Zahn, D. Chem. - A Eur. J. 2010, 16, 8349–8354.

[10] Rao, R. P.; Adams, S. Phys. Status Solidi 2011, 208, 1804–1807.

[11] Chen, M.; Prasada Rao, R.; Adams, S. Solid State Ionics 2014, 268, 300–304.

[12] Chen, M.; Adams, S. J. Solid State Electrochem. 2015, 19, 697–702.

[13] Chen, M.; Rao, R. P.; Adams, S. Solid State Ionics 2014, 262, 183–187.

[14] Yubuchi, S.; Teragawa, S.; Aso, K.; Tadanaga, K.; Hayashi, A.; Tatsumisago, M. J. Power Sources 2015, 293, 941–945.

[15] Boulineau, S.; Tarascon, J.-M.; Leriche, J.-B.; Viallet, V. Solid State Ionics 2013, 242, 45–48.

[16] Yu, C.; van Eijck L.; Ganapathy, S.; Wagemaker, M. *Electrochimica Acta* 2016, 215, 93–99.

[17] Dedryvère, R.; Foix, D.; Franger, S.; Patoux, S.; Daniel, L.; Gonbeau, D. J. Phys. Chem. C 2010, 114, 10999–11008.

[18] El Ouatani, L.; Dedryvère, R.; Siret, C.; Biensan, P.; Reynaud, S.; Iratçabal P.; Gonbeau, D. J. Electrochem. Soc. 2009, 156, A103-A113.

[19] Dahéron, L.; Dedryvère, R.; Martinez, H.; Ménétrier, M.; Denage, C.; Delmas, C.; Gonbeau, D. Chem. Mater. 2008, 20, 583–590.

[20] A. Sakuda, A. Hayashi, M. Tatsumisago, *Chem. Mater.* 2010, 22, 949-956.

[21] A. Sakuda, A. Hayashi, T. Ohtomo, S. Hama, M. Tatsumisago, *J. Power Sources*, 2011, 196, 6735-6741

[22] W. D. Richards, L. J. Miara, Y. Wang, J. C. Kim, G. Ceder, *Chem. Mater.* 2016, 28, 266-273.

[23] Wagner, C. D.; Riggs, W. M.; Davis, L. E.; Moulder, J. F.; Muilenberg, G. E. Handbook of X-ray photoelectron spectroscopy; 1981.

[24] Franke, R.; Chassé, T.; Streubel, P.; Meisel, A. *J. Electron Spectros. Relat. Phenomena* 1991, 56, 381–388.

[25] Ji, X.; Lee, K. T.; Nazar, L. F.; *Nat. Mater.* 2009, 8, 500−506.

[26] Vizintin, A.; Lozinšek M.; Chellappan, R. K.; Foix, D.; Krajnc, A.; Mali, G.; Drazic, G.; Genorio, B.; Dedryvère, R.; Dominko, R.; *Chem. Mater.* 2015, 27, 7070-7081.

[27] H. Visbal, Y. Aihara, S. Ito, T. Watanabe, Y. Park, S. Doo, *J. Power Sources* 2016, 314, 85-92.

[28] Takada, K.; Aotani, N.; Iwamoto, K.; Kondo, S.; *Solid State Ionics* 1996, 86-88, 877-882.

[29] Tatsumisago, M.; Mizuno, F.; Hayashi, A. *J. Power Sources* 2006, 159, 193-199.

[30] F. Han , T. Gao , Y. Zhu , K. J. Gaskell, C. Wang, *Adv. Mater.* 2015, 27, 3473−3483.

[31] I. Tarhouchi, V. Viallet, P. Vinatier, M. Ménétrier, *Solid State Ionics* 2016, 296, 18-25.
[32] Wenzel, S.; Weber, D. A.; Leichtweiss, T.; Busche, M. R.; Sann, J.; Janek, J. ; *Solid State Ionics* 2016, 286, 24–33.
[33] Wenzel, S.; Randau, S.; Leichtweiß, T.; Weber, D. A.; Sann, J.; Zeier, W. G.; Janek, J.; *Chem. Mater.* 2016, 28, 2400-2407.
[34] Li, W. J.; Hirayama, M.; Suzuki, K.; Kanno, R.; *Solid State Ionics* 2016, 285, 136-142